# Scale-up and Modeling of Fixed-Bed Reactors for Catalytic Phenol Oxidation over Adsorptive Active Carbon

Somsaluay Suwanprasop, Athanasios Eftaxias, Frank Stüber, Isabelle Polaert, Carine Julcour-Lebigue, Henri Delmas

# SCALE UP AND MODELLING OF FIXED BED REACTORS FOR THE CATALYTIC PHENOL OXIDATION OVER ADSORPTIVE ACTIVE CARBON

Somsaluay Suwanprasop[1], Athanasios Eftaxias[2], Frank Stüber[2]*, Isabelle Polaert[1], Carine Julcour-Lebigue[1], Henri Delmas[1]

[1] *Laboratoire de Génie Chimique, UMR CNRS 5503, 5 rue Paulin Talabot, 31106 Toulouse, France.*

[2] *Departament d'Enginyeria Química, ETSEQ, Universitat Rovira i Virgili, Av. dels Països Catalans, 26, 43007 Tarragona, Catalunya, Spain.*

## Abstract

The wet air oxidation of phenol over a commercial active carbon catalyst has been studied in laboratory and pilot plant Fixed Bed Reactors at mild temperatures and oxygen partial pressures of 120-160 ºC and 0.05-0.2 MPa, respectively. The performance of the Fixed Bed Reactors has been assessed and compared to each other for both up-and downflow operation mode. Depending on the flow mode and reactor scale, distinct phenol destruction rates have been observed in the experiments. A series of batch experiments are carried out to obtain phenol removal kinetics, which are subsequently implemented in the modelling of the pilot Fixed Bed Reactor. A one-dimensional non-isothermal Piston Dispersion model is developed to describe in detail the interplay of reaction kinetics, gas-liquid hydrodynamics and heat and mass transfer in both flow directions. The model predicts reasonably well the experimental data, thus allowing for a thorough explanation of the observed pilot reactor performance.

**Keywords:** CWAO, Phenol, Active Cabon Catalyst, Fixed Bed Reactors, Scale up, Modeling

## 1. Introduction

The increasing release of organic pollutants contained in many industrial end stream effluents has been the driving force for developing alternative effluent treatments prior to their discharge to conventional biofilters or sewage plants. A suitable destruction of such pollutants is Catalytic Wet Air Oxidation (CWAO) at mild operating conditions and attractive process economics[1]. Recently, catalysts with improved stability in CWAO of phenol and various substituted phenols have been developed either based on noble metals[2], mixed oxides[3] or Active Carbon (AC)[4]. By employing AC, unit operations of adsorption and reaction are naturally combined in an adsorptive oxidation reactor. CWAO over AC becomes especially attractive when integrated in adsorption-oxidation cycles[5] or biological end-treatments[6], as complete mineralisation of organic pollutants by CWAO alone is no longer required.

In most CWAO studies[4, 7-9], Fixed Bed Reactors (FBRs) have been preferred over slurry or fluidised bed reactors. Also, several aromatic pollutants show the ability to undergo homogeneous condensation reactions via oxidative coupling[10] and large catalyst to liquid ratios as in fixed bed reactor are required to limit these side reactions and fast catalyst deactivation[9]. To properly design and operate industrial CWAO units, pilot reactor performance and modelling of continuous fixed bed reactors must be assessed. At present, most of the work on CWAO has been focused on catalysts and kinetic analysis than on understanding the overall reactor performance[11]. The studies that are related to process analysis often cover only a specific reactor aspect[8-9], simplify reactor modeling[12] or do not provide any experimental results to support model predictions[13].

Thus the aim of this work is to thoroughly investigate the CWAO of phenol over AC in both a small scale and pilot plant FBR and to carry out detailed reactor modelling to understand the complex interplay of reaction kinetics, intraparticle and interphase heat and mass transfer and gas-liquid hydrodynamics.

## 2. Experimental

### *2.1 Materials*

Deionised water and analytical grade phenol (Aldrich) are used to prepare 5 g/l phenol solutions. The oxidant was either compressed high purity air (Carburos Metalicos, Linde Gas) or pure oxygen mixed with pure nitrogen (Linde Gas). AC ($d_p$= 1.5 or 2.5 mm) is purchased from Merck (Refs 2514 & 2518, ash content 3.75%, B.E.T specific surface area 990 $m^2/g$, pore volume 0.55 $cm^3/g$ and mean pore diameter of 1.4 nm). Phenol adsorption tests under air atmosphere have shown a maximum capacity of 370 $mg_{Ph}/g_{AC}$ at 20ºC. Prior to experiments in small scale TBR, the AC particles are crushed and sieved to obtain the 0.3-0.7 mm fraction. Each sample is washed, dried at 110ºC for 12 h and stored under inert atmosphere at room temperature. For the pilot plant experiments and batch kinetic study, the 1.5 mm particles are sieved to get the 1.25-1.6 mm fraction (D[4,3] = 1.0 mm by Mastersizer 2000, Malvern).

### *2.2 Catalytic reactors and operating conditions used*

Table 1 gives the range of operating conditions used in the kinetic and scale-up studies.

**Batch Basket Reactor**

For the determination of intrinsic kinetic parameters, batch phenol oxidation is performed in a stirred autoclave (Parr Instruments) using the 1.25-1.6 mm fraction of AC to reduce fast and continuous catalyst deactivation as previously reported with powder[9]. Details on experiments (see also table 1) and results are presented elsewhere[14].

**Laboratory Fixed Bed Reactor**

CWAO of 5 g/l phenol solutions has first been conducted in a small laboratory reactor placed in a temperature-controlled oven (±1 ºC). The reactor is filled with 6.6-7 g of AC retained between two sintered metal disks. A detailed reactor scheme is available elsewhere[15]. The oxidation tests have been performed in downflow and upflow mode at constant temperature

(120, 140, 160 ºC) and oxygen partial pressure (0.1, 0.2 MPa). The air flow rate is set at 2.4 ml/s (STP) to assure 100-250% oxygen excess for complete phenol oxidation. The liquid flow rates selected correspond to space-times and liquid superficial velocities of 0.04-0.6 h and 0.04 to 0.55 mm/s, respectively. At a fixed liquid flow rate, the reactor is rapidly heated up, while saturation of AC bed with phenol and oxidation reactions require 20 h to reach steady state. To obtain conversion-space time profiles, the liquid flow rate is varied . After each change, the evolution of phenol concentration is monitored to detect the new steady state of reaction, which, depending on the liquid flow rate, is achieved within 2-4 h. The liquid phase composition is immediately analysed by taking three samples at steady state conditions. The experimental error in the phenol and COD concentrations is evaluated to be of ± 5%.

**Pilot Plant Reactor**

A pilot reactor of 2.5 cm in diameter and 120 cm in length (see figure 1) has been designed, constructed and tested. The reactor tube is filled with 325 g of AC. The reactor tube is covered with a double jacket annular heater, where hot thermal oil is pumped through at a high flow rate at 120 to 160 ºC. Non-isothermal reactor operation results from feeding the gas-liquid mixture at room temperature. The oxygen partial pressure is ranged from 0.05 to 0.2 MPa, the liquid space-time from 0.1 to 0.7 h corresponding to superficial velocities of 0.3 to 2 mm/s, and the inlet gas superficial velocity from 5 to 25 mm/s. The pilot unit is designed to operate in up- and downflow mode of gas-liquid flow by means of 5 three-way valves located along the gas and liquid circuits (see figure 1).

Several temperature sensors and sampling valves have been mounted along the reactor to measure concentration and temperature axial profiles under non-isothermal conditions and wall to bed heat transfer in both flow modes. Liquid sampling is also done after the gas-liquid separator. To vary the oxygen partial pressure, either the total pressure (measured in the gas outlet of the separator and controlled by a PID), and/or the composition of the $O_2/N_2$ inlet

mixture are adequately adjusted. Gas and liquid flow rates are set and measured by mass-flow controllers and a precision liquid pump and balance, respectively.

The start up of oxidation experiments in the pilot plant consists in saturating first the AC during 10 h under nitrogen atmosphere at reaction temperature. Once the phenol break through is observed, air or $O_2/N_2$ mixture is fed instead of nitrogen. Phenol concentration at the reactor outlet is measured each 30 minutes until steady state of reaction is reached (after 1 to 4 h depending on the operating conditions). Then, the liquid or gas flow rate is set to a new value. In this way, about 50 experiments have been carried out to investigate the influence of temperature, oxygen pressure, gas and liquid flow rate as well as flow direction on reactor performance. During the experiments, liquid and gas flow rates and temperatures are monitored on-line using a microcomputer data acquisition system.

### *2.3 Analysis*

Exit liquid samples are analysed with a HPLC using a $C_{18}$ reverse phase column (Spherisob ODS-2 or ProntoSIL C18 AQ) to obtain concentration of phenol and intermediates. The separation is achieved with a mobile phase of variable composition programmed at 1 ml/min, using as eluants acidified deionised water and acetonitrile or methanol. Compounds are detected with UV at a wavelength of 210 nm (intermediates) and 254 nm (phenol). A standard mixture of phenol and oxidation products is periodically tested. The liquid stream is also analysed for the remaining COD.

## 3. Model Development

### *3.1. Kinetic Model*

In agreement with previous kinetic studies[15], a simple power law is convenient to accurately describe the phenol destruction over AC assuming a first order of phenol, while the oxygen order has to be determined by the optimisation algorithm. The first order of phenol is also

confirmed when plotting the logarithm of phenol concentration as a function of time (not shown here). The following rate equation can thus be proposed:

$$R_{phenol} = -k_0 \, exp\left(\frac{-E}{RT}\right) C_{Ph} \, x_{O_2}^{\alpha} \qquad (1)$$

The values of the Weisz modulus ($0.45 < \phi' < 1.5$) at initial time and oxygen being the limiting reactant, indicate that the reaction occurs in the intermediate diffusion regime. The intrinsic kinetics of phenol oxidation is thus derived using a batch reactor model that accounts for transient diffusion of both oxygen and phenol inside the catalyst pores[16]. In the model, spherical geometry is assumed with D[4,3] = 1.0 mm as reference diameter and a tortuosity value of 3 to evaluate the effective diffusivities of oxygen and phenol.

A 0.5 oxygen order has been identified to match best the phenol concentrations obtained at 140 ºC and 0.1 to 0.35 MPa of oxygen partial pressure. The activation energy and frequency factor for phenol oxidation are respectively 74 kJ/mol and $3.75 \cdot 10^5$ $m^3$ $s^{-1}$ $kg^{-1}$.

### *3.2. Reactor Model*

The present non-isothermal model is based on previous work[13, 15]. The model parameters of interest are the axial liquid phase temperature and the axial liquid phase concentrations of dissolved oxygen and organic compounds, in particular the conversion of the phenol reactant. The model reflects the complex interplay of reaction kinetics, gas-liquid hydrodynamics and heat and mass transfer on both the pellet and reactor length scale. Splitting of the total liquid hold-up into stagnant and dynamic parts are considered, as well as partial wetting for downflow mode, to establish weighted effectiveness factors that address both the gas limiting and liquid limiting reactant situation. Furthermore, to simulate non-isothermal reactor operation, two limiting cases of water vaporisation are described, i.e. instantaneous vapour-liquid equilibrium and progressive axial saturation of the gas phase with water.

On the whole, the model accounts for:

- Static and dynamic liquid portions.
- Constant partial catalyst wetting in trickle flow regime throughout the reactor.
- Axial dispersion in the dynamic liquid phase.
- Pore diffusion and gas-liquid and liquid-solid mass transfer.
- Axial concentration and temperature gradients, but no radial gradients ($D_R/d_p$=25).
- Heat transfer between catalytic fixed-bed and reactor wall (at constant wall temperature).
- Instantaneous water vapour-liquid equilibrium or mass transfer limited axial saturation of gas phase with water.

The following assumptions have been made in the model development:

- Stable catalyst activity.
- Complete internally wetted catalyst pores.
- No temperature gradient between gas, liquid and catalyst.
- Negligible pressure drop, i.e. the total pressure is constant.
- Ideal gas phase behaviour.
- Organic reactants are non-volatile.

For simulations presented in following sections, only complete mineralisation of reacted phenol to $H_2O$ and $CO_2$ is considered, as intermediates represent in most cases less than 20% of total COD and do not significantly increase at high phenol conversion.

**Pellet scale model**

For simultaneous diffusion–reaction of reactants and products within the liquid filled pores, the following mass balance equation has been solved, assuming spherical symmetry:

$$\frac{1}{r^2}\frac{d}{dr}\left( r^2 D_j^{eff} \frac{d C_j}{dr} \right) + \rho_p R_j = 0 \qquad (2)$$

with boundary conditions at r = 0:

$$\left.\frac{dC_j}{dr}\right|_{r=0} = 0 \qquad (3)$$

and r= $r_p$:

$$C_j\big|_{r=r_p} = C_j^*$$

$$D_j^{eff}\left.\frac{dC_j}{dr}\right|_{r=r_p} = k_{jls}^{d}\, f_d\,(C_j^{d} - C_j^{*}) + k_{jls}^{s}\, f_s\,(C_j^{s} - C_j^{*}) + \Big[k_{gs}(1-f)(C_{O_2}^{g} - H\,C_{O_2}^{*})\Big]_{\substack{only \\ for\ O_2}} \tag{4}$$

Eq.(4) accounts thus for the effect of stagnant liquid pockets and partial wetting without the need of assuming a limiting reactant. However, this approach considers a uniform concentration of reactants on the catalyst surface (required by the use of a one dimensional-diffusion model) assuming infinite radial diffusion. Eq.(4) for the boundary condition at the particle surface is based on the reactant concentration j in the liquid bulk or gas bulk, which have to be calculated by the reactor scale model. To link the fluid and surface concentration of each compound j, a weighted effectiveness factor that accounts for the fluid-solid mass transfer resistance is defined for each of the fraction of the pellet surface in contact with the liquid or gas phases:

$$\eta_j^{d} = \frac{3k_{jls}^{d}\, f_d\,(C_j^{*} - C_j^{d})}{r_p\,\rho_p\,R_j^{*}}$$

$$\eta_j^{s} = \frac{3k_{jls}^{s}\, f_s\,(C_j^{*} - C_j^{s})}{r_p\,\rho_p\,R_j^{*}}$$

$$\eta_{O_2}^{g} = \frac{3k_{gs}(1-f)(HC_{O_2}^{*} - C_{O_2}^{g})}{r_p\,\rho_p\,R_{O_2}^{*}} \tag{5}$$

**Reactor scale model**

Axial dispersion in the liquid phase can alter the reactor performance and the one-dimensional Piston Dispersion Exchange (PDE) model has been used. The gas phase is assumed to be in plug flow. If catalyst wetting is not complete as in trickle bed regime, the following equation results for the oxygen gas phase concentration:

$$\frac{d(u_g C_{O_2}^{g})}{dz} + (k_L a)\left(\frac{C_{O_2}^{g}}{H} - C_{O_2}^{d}\right) - \eta_{O_2}^{g}\rho_b R_{O_2}^{*} = 0 \tag{6}$$

The dynamic liquid concentrations are given by the following mass balance equation, which includes axial dispersion:

$$-D^{ad}\,\varepsilon_{ld}\frac{d^2C_j^d}{dz^2}+\frac{d(u_lC_j^d)}{dz}+(ka)_{jll}(C_j^d-C_j^s)-\eta_j^d\,\rho_b\,R_j^*-\left[k_L\,a(\frac{C_{O_2}^g}{H}-C_{O_2}^d)\right]_{\substack{only\\ for\,O_2}}=0 \tag{7}$$

For the stagnant liquid pockets that may exist on the reactor length scale, the convection term drops out and algebraic equations describe the stagnant liquid concentrations:

$$(ka)_{jll}(C_j^d-C_j^s)+\eta_j^s\,\rho_b\,R_j^*=0 \tag{8}$$

Finally, based on Van Gelder et al.[17], the energy balance for the pseudo-homogeneous gas-liquid fluid incorporating water evaporation and bed to wall heat transfer gives:

$$(u_l\rho_lc_{pl}+u_g\rho_gc_{pg})\frac{dT}{dz}+\frac{\varphi}{A}\Delta H^v-\rho_b\Sigma\,r_i^{ap}(-\Delta H_i)+\frac{h_wA}{V_R}(T-T_w)=0 \tag{9}$$

The apparent rate of the $i^{th}$ reaction ($r_i^{ap}$) is calculated from stoichiometry and the compound overall reaction rates ($\eta_jR_j$). Here as mentioned before only one reaction of complete oxidation is considered. The thermal fluid being circulated at a high flow rate through the thermally isolated double jacket the reactor wall temperature remains constant.

The water evaporation rate ($\varphi$) per unit reactor length is determined assuming that the gas stream reaches either instantaneously liquid-vapour equilibrium or is progressively saturated while flowing through the catalytic fixed bed.

Denoting the total molar gas flow rate by $\dot{n}_T^g$ and the water vapour molar flow rate by $\dot{n}_{H_2O}^g$, then the following equality must be always fulfilled in case of instantaneous saturation of the gas stream with water vapour:

$$\frac{\overset{g}{\dot{n}}_{H_2O}}{\overset{g}{\dot{n}}_T} = \frac{\overset{g}{P}_{H_2O}(T)}{P_T} \tag{10}$$

If the mass transfer of water from the liquid to the gas phase is not fast enough, the gas phase becomes progressively saturated along the axial reactor coordinate, leading to:

$$\frac{1}{A}\frac{d\overset{g}{\dot{n}}_{H_2O}}{dz} + k_G a\left(\overset{g}{C}_{H_2O} - \frac{\overset{g}{P}_{H_2O}(T)}{RT}\right) = 0 \tag{11}$$

$$\overset{g}{C}_{H_2O} = \frac{\overset{g}{\dot{n}}_{H_2O}}{\overset{g}{\dot{n}}_T}\frac{P_T}{RT} \tag{12}$$

The total system pressure $P_T$ being only marginally affected by the pressure drop throughout the bed under the giving operating conditions is considered constant in the model.

Neglecting incomplete cold gas saturation, it follows:

$$\overset{g}{\dot{n}}_{H_2O} = \left(\overset{g}{\dot{n}}_{H_2O}\right)_{inlet} + \int_0^z \varphi(z)\,dz \tag{13}$$

$$\overset{g}{\dot{n}}_T = \left(\overset{g}{\dot{n}}_T\right)_{inlet} + \int_0^z \varphi(z)\,dz \tag{14}$$

The fluid temperature and the total molar gas and liquid flow rates undergo changes along the fixed-bed reactor length and the gas and liquid superficial velocities have to be adjusted accordingly. For the gas phase, the axial variation of the superficial velocity is calculated assuming ideal gas behaviour:

$$u_g = \frac{\dot{V}_g}{A} = \frac{\overset{g}{\dot{n}}_T RT}{P_T A} \tag{15}$$

differentiating Eq.(16) leads to:

$$\frac{du_g}{dz} = \frac{RT}{P_T A}\varphi + \frac{\overset{g}{\dot{n}}_T R}{P_T A}\frac{dT}{dz} \tag{16}$$

For the dynamic liquid phase, the change in superficial velocity is calculated respectively, using the liquid density of pure water:

$$\frac{du_l}{dz} = \frac{d}{dz}\left(\frac{\dot{m}_l}{A\rho_l}\right) = \frac{\dot{m}_l}{A}\frac{d}{dT}\left(\frac{1}{\rho_l}\right)\frac{dT}{dz} + \frac{1}{A\rho_l}\frac{d\dot{m}_l}{dz} \tag{17}$$

The boundary conditions for the reactor scale model are as follows.

At the reactor entrance (z=0):

$$C_{O_2}^{g} = \left(C_{O_2}^{g}\right)_{inlet} \tag{18}$$

$$u_l\left(C_j^d\right)_{inlet} = u_l\, C_j^d\Big|_{z=0^+} - \varepsilon_{ld}\, D^{ad}\,\frac{\partial C_j^d}{\partial z} \tag{19}$$

$$T = T_{inlet} \tag{20}$$

At the reactor outlet ($z=L_R$):

$$\frac{\partial C_j^d}{\partial z} = 0 \tag{21}$$

### *3.3. Physical properties, hydrodynamic and mass and heat transfer parameters*

Pure water and air or gas mixture properties are considered for the bulk liquid and gas phases. Water and gas heat capacities, water heat of evaporation, heat of phenol combustion, water vapour pressure, water density as well as phenol diffusion coefficients have been obtained from data or methods included in Reid et al.[18]. Dissolved oxygen diffusion coefficient and Henry constants for oxygen solubility in water are taken from Diaz et al.[19] and Himmelblau[20], respectively. Table 2 gives values of these parameters calculated for the temperature range studied.

The quality of prediction of the packed-bed model depends primarily on the accuracy of the involved model parameters. Kinetic parameters have been assessed from suitable

experiments[14]. For the other key parameters, the available literature correlations have been examined to select appropriate values. However, this turns out to be a difficult task since there can exist a very large dispersion between the results calculated from the specific correlations. Hydrodynamic and transport parameters strongly depend on the nature of the gas-liquid flow through the bed. For cocurrent two-phase upflow and bubble flow regime, the liquid phase is continuous and the packed-bed column operates with high liquid holdups and fully wetted pellets. External mass transfer and axial dispersion are thus gaining importance. When the packed-bed is operated in trickle downflow regime, the gas phase becomes the continuous phase and partial wetting of pellets may occur. In this situation, external mass transfer and axial dispersion can be less influent, whereas the pellet wetting efficiency is thought to be crucial for the reactor conversion. Table 3 lists both the literature correlations selected and a set of values of key model parameters.

### *3.4. Numerical solution*

The PDE model in combination with the classical pore diffusion model is applied to describe the performance of the packed-bed pilot reactor. A sequential approach is performed to numerically solve the corresponding equation system.

The pellet and reactor scale models lead to a set of algebraic-differential equations that involve non-linear reaction rates. To solve these model equations with boundary constraints, the robust numerical method of orthogonal collocation on finite elements has been used (Finlayson[21]). In most situations, 8 collocation points have been sufficient to obtain readily model convergence both for reactor and pellet length scale with only one finite element.

## 4. Results and discussion

### *4.1. Phenol oxidation over AC in laboratory FBRs*

**Catalytic Performance of AC in Trickle Bed Reactor.**

The phenol conversion space-time profiles obtained in downflow operation are given in Figure 2 for oxygen partial pressures and temperatures of 0.1, 0.2 MPa and 120, 140, 160 ºC, respectively. The phenol destruction is seen to improve strongly with increasing temperature, pressure and liquid space-time. At low conversion of phenol, mineralisation of reacted phenol to $CO_2$ and $H_2O$ is almost complete, while the difference between phenol and COD conversion becomes larger as the phenol conversion increases. At 160 ºC and 0.2 MPa, phenol and COD destruction beyond 99% and 85%, respectively, are achieved for space-times greater than 0.4 h. Compared to recently developed catalysts[11], the active carbon studied displays thus a comparable or even better catalytic performance in phenol CWAO at 160 ºC but significantly lower oxygen partial pressure of 0.2 MPa.

The main intermediates detected are 4-hydroxybenzoic acid (due to some interaction with AC, 4-hydroxybenzoic acid being usely not found with other catalysts), benzoquinone, maleic, formic and acetic acids as well as traces of hydroquinone, catechol and oxalic acid. The AC catalyst exhibited accumulation of refractory acetic acid, which accounts for 15% of the liquid phase COD remaining at the highest phenol conversions.

**Comparison of Trickle Bed Reactor and Flooded Bed Reactor.**

Gas-liquid hydrodynamic and mass transfer parameters are key parameters for understanding the performance of FBRs. Here, it is shown with the help of three-phase reactor flow maps that the TBR always operated in the trickling regime. Due to its low solubility, oxygen though in large excess is the limiting reactant as calculated according to Khadilkar et al.[22].

In the trickle flow regime, the external liquid hold-up takes small values of around 0.1 and the catalyst wetting efficiency is estimated to range between 0.25 and 0.5 at the liquid flow rates used[23, 24]. Since gas-solid mass transfer is generally one or two order of magnitude

higher (see Table 3) than that at the liquid-solid interface, the liquid filled pores that connect to the 'dry' particle surface are always saturated with oxygen. Partial wetting in downflow mode should then positively affect the catalyst performance. This trend is clearly confirmed in Figure 3, which compares the reactor performance for both fully wetted upflow mode and partially wetted downflow mode. The downflow mode occurring in the kinetic controlled regime yields substantially lower phenol outlet concentrations (i.e. higher phenol conversions) in all conditions tested. The fully wetted upflow mode is therefore limited by the presence of gas-liquid mass transfer limitations of oxygen and probably some degree of axial dispersion at the lowest liquid flow rates.

### *4.2. Scale-up of phenol oxidation over AC*

The phenol oxidation has been also performed in a jacketed pilot reactor to scale-up the process and assess its performance under eventually mass transfer limited and non-isothermal conditions.

The experimental standard procedure as described in chapter 2.2 includes steps of reactor start-up, steady state of reaction and regular control of catalyst activity. Steady state conditions of reaction are verified through transient sampling. Transient periods to reach steady state (from 1.5 to 4 h) mainly depend on the liquid flow rate selected as well as the operating conditions of the previous run, leading to different preliminary adsorption times. Catalyst activity has been regularly checked at the following standard conditions of $T_{oil}$=140 ºC, $F_L$=1 kg/h, $Q_G$=100 Nl/h and $P_{O2}$=0.12 MPa. No deactivation is observed at 120 and 140°C after more than 300 hours of operation corresponding to 5 g of phenol treated per g of AC. However, at the highest reaction temperature of 160 ºC, the catalyst activity is quickly reduced by 20% after a few runs of 30 h in total.

In the experimental series, the four main operating parameters ($T_{oil}$, $P_{O2}$, $u_l$ and $u_g$) and flow direction have been investigated over a wide range of operating conditions (see Table 1). In this way, a large set of steady state data has been obtained in the pilot plant reactor. The obtained phenol conversions are displayed as a function of liquid space-time in Figures 4, 5 and 6 for different pressures, temperatures and gas velocities, respectively.

The most striking observation is that, contrary to the small FBR experiments, both upflow and downflow mode lead to very similar phenol conversions at any condition. This result is confirmed by the standard deviation between upflow and downflow that is calculated to about 12% without any correlation to the four operating parameters studied. Another important difference is found for the distribution of reaction intermediates. Phenol oxidation in the pilot FBR results in much less maleic acid but much more malonic and oxalic acids. Also, formic acid concentration is double, whereas acetic acid concentration is 4 times less. Only the concentrations of aromatic compounds remain similarly low in the two FBRs.

As expected from the batch kinetic study, phenol conversion significantly increases with partial oxygen pressure (Figure 4) and temperature (Figure 5) in rough agreement with kinetics. On the other hand gas velocity has only a very small effect (Figure 6) in both operation modes. If in downflow external mass transfer coefficients are known to depend mostly on liquid velocity, a more marked positive effect would be expected in upflow mode. Actually the poor effect of gas flow rate could be explained either by marginal effect of external mass transfer in quasi kinetic control or by its balanced influences on mass transfer and on vaporisation. This situation of different external mass transfer and its effect on the FBR performance will be detailed in chapter 4.3.

On the whole, it can be concluded that the scale-up of phenol CWAO over AC based on simple liquid space-time analogy would lead to erroneous reactor design, which clearly

highlights the need for developing detailed reactor models to predict the reactor performance on different reactor scales.

### *4.3. Prediction of pilot plant reactor performance*

The pilot reactor data has been thoroughly analysed with the detailed PDE model developed in section 3.2. In addition to physicochemical properties, thermodynamic and kinetic data, the packed-bed reactor model requires the input of several key parameters such as wall to bed heat transfer coefficient, liquid side and gas side volumetric mass transfer coefficients, both for oxygen absorption and water vaporisation, as well as liquid-solid mass transfer coefficient. For trickle bed simulation the situation is even more complex, including partial catalyst wetting. The accurate prediction of all these parameters is a critical task for successful reactor modelling. Various correlations exist for the main model parameters, although a dramatic spreading up to two orders of magnitude can result from their application, as in the case of the volumetric mass transfer coefficient. A large difference is also found for the liquid axial dispersion coefficient in upflow operation. Moreover, for the most refined trickle bed model, some model parameters can not even be estimated due to lack of specific correlations.

In the case of phenol CWAO, heat transfer and axial temperature profiles may be analysed separately due to relatively high heat transfer (small tube diameter), very low heat production by reaction (diluted phenol), and moderate heat consumption for water vaporisation. As shown in Figure 7, the predicted temperatures fit well with the experimental temperature profiles when using the correlation of Sokolov et Yablokova[25] in upflow and a modified correlation of Mariani et al.[26] in downflow (divided by 2). It clearly appears that upflow provides superior wall to bed heat transfer conditions (steeper temperature profiles), nevertheless even in downflow the reactor temperature reaches the wall temperature after

about 30 cm of the catalytic fixed bed. Thus, as a first approximation, the reactor can be considered to operate quasi isothermally.

The situation of gas-liquid upflow operation being less complex will be first examined. The sensibility of the reactor performance to oxygen mass transfer and water vaporisation is not straightforward. In the non-isothermal reactor zone (first 30 cm of the fixed bed) the water vapour pressure increases exponentially and the induced water vaporisation reduces gradually the oxygen partial pressure in the gas phase and at the same time increases phenol concentration in the remaining liquid and the liquid space-time. The effect of vaporisation is rarely accounted for in modelling and therefore, two vaporisation rates have been implemented and compared: either instantaneous vapour-liquid equilibrium, i.e. infinitely fast vaporisation, or mass transfer limited vaporisation, involving the gas side volumetric mass transfer coefficient ($k_G a$). This parameter is not well known neither for upflow nor for downflow, where it has been reported to be at least equal to the liquid side mass transfer coefficient (Gianetto and Silveston[27]).

To assess the influence of water vaporisation on upflow reactor performance, a set of simulations with $k_G a = k_L a$, $k_G a = 5 \times k_L a$ and $k_G a$ = infinite (equilibrium) has been carried out. The Saada[28] correlation is used to calculate $k_L a$ and in the following the obtained $k_L a$ values are multiplied and divided by 5. The results of the sensitivity study are summarised in Table 4 for the reference conditions of $T_{oil}$=140 ºC, $Q_G$=100 Nl/h and $P_{O2}$=0.12 MPa. A lower liquid flow rate of $F_L$= 0.5 kg/h has been selected both to achieve a larger phenol conversion and to test the effect of axial dispersion in the liquid phase.

For the axial dispersion coefficients studied, only a limited change of outlet phenol conversion (always less than 7%) has been observed in the simulation runs. Thus, it can be concluded that axial dispersion effects do not play a significant role for phenol conversion under the given operating conditions. Simulation results are first compared with the reference

case ($k_La$ from Saada[28], instantaneous equilibrium and axial dispersion from Stüber[29]) and then with the experimental conversion (last column of table 4). With respect to the gas-liquid mass transfer, at high $k_La$ values (5 times higher), the vaporisation rate ($k_Ga$) has nearly no influence on conversion increasing slowly from 30.1 to 35.3%, although the experimental conversion is overestimated by 23 to 27.8%. The situation becomes very different at low $k_La$ values (5 times smaller) that can generate very large underestimation of conversion up to -85% depending on the vaporisation rate ($k_Ga$). This suggests that the gas-liquid mass transfer in upflow operation is only moderately limiting the reactor conversion. The Saada[28] correlation giving the best agreement with experimental data will be further used in the model predictions.

Figures 8 a and b show profiles of experimental exit phenol concentration and corresponding simulations for upflow operation. It is seen that the best agreement with experimental data is found for a relation of $k_L/k_G$ =5. Nevertheless, in the range of conditions studied in this work, it appears that the rate of water evaporation does not significantly change the outlet concentration and vapour-liquid equilibrium could be assumed for simplicity.

However, the slightly positive effect of increasing gas velocity on phenol conversion observed experimentally in upflow mode could not be checked by the model. Best model predictions (if $k_Ga = k_La$) show nearly no influence of gas velocity, or an increase of outlet phenol concentration due to higher water vaporization flux.

The simulation of the trickle bed reactor is even more complex involving partial catalyst wetting, which is found to have a strong impact on reactor performance as shown in Table 5. As soon as full wetting is not assumed ($f < 1$), mass transfer to the dry zone becomes extremely fast and oxygen mass transfer limitation vanishes. This large overestimation of the effect of catalyst wetting in the model is due to the assumption of uniform concentration at the catalyst surface whatever wet or dry. As a consequence, there is no sensitivity to the value of

the external wetting efficiency, the only important hypothesis being either fully or partially wetted conditions. Indeed, there is no simple way to account for multidirectional pore diffusion resulting from non-uniform oxygen transfer to the catalyst surface. The use of different overall effectiveness factor for each zone could be a solution, but it would be very difficult to implement when limitations both due to the liquid and dissolved gaseous reactant are present.

The volumetric mass transfer coefficient remains then one key model parameter. The correlation of Morsi[30] gives a lower value than that for upflow mode in similar operating conditions[31, 32]. In Figure 9, experimental downflow data are thus compared to the two models of either full or partial catalyst wetting. In general, the experimental data lie mostly in between the two simulations, oxygen mass transfer being too fast with any partial wetting and too slow at full wetting.

These simulations results indicate that the opposite roles of oxygen mass transfer and water vaporisation are not simply balanced and may have different importance depending on the reaction and hydrodynamic conditions. This situation is not often addressed in modelling of FBR involving oxidation in the liquid phase, though corresponding to typical industrial condition for CWAO and thus should deserve further research work.

## 5. Conclusions

The performance of laboratory and pilot fixed bed reactors has been assessed for the CWAO of phenol over active carbon at mild conditions. The laboratory fixed bed reactor performs high phenol and COD destructions of 99% and 85% in downflow mode at 160 ºC, 0.2 MPa of oxygen partial pressure and space-time of 0.4 h. Upflow mode, however, leads to lower phenol outlet conversions due to fully wetted catalyst pellets and stronger gas-liquid mass transfer limitations. Contrary, in the pilot plant reactor, similar outlet phenol concentrations

have been obtained for both gas-liquid flow directions over the whole range of operating conditions studied. Moreover, the distribution of partial oxidation products is found to depend on the reactor size. In view of the distinct reactor performance, it is clear that the scale-up of fixed bed reactor for phenol CWAO based on mere space-time analogy can not be recommended.

The pilot plant reactor has been simulated by a complex non-isothermal 1D-PDE model, which includes different vaporisation rates during non-isothermal operation. The effect of water vaporisation on the reactor performance is shown to be important, although it is rarely included in modelling of CWAO reactors. On the whole, the model predictions match conveniently the experimental pilot plant data for both flow directions. The model developed represents with adequate precision the complex interplay of reaction kinetics, hydrodynamics and mass transfer phenomena assuming the absence of radial temperature and concentration gradients. It is thus a very useful tool to support the proper design of industrial CWAO units and can avoid the drawbacks of the too simple space-time approach.

**Nomenclature**

| | |
|---|---|
| $A$ | reactor section area ($m^2$) |
| $C_j$ | concentration of compound j ($mol/m^3$) |
| $C^g_{H2O}$ | gas phase concentration of water vapour ($mol/m^3$) |
| $c_{pl}$ | liquid heat capacity ($J\ kg^{-1}\ K^{-1}$) |
| $c_{pg}$ | gas heat capacity ($J\ kg^{-1}\ K^{-1}$) |
| $D_j$ | diffusion coefficient of compound j ($m^2/s$) |
| $D_j^{eff}$ | effective diffusion coefficient of compound j ($m^2/s$) |
| $D^{ad}$ | axial dispersion coefficient ($m^2/s$) |
| $E$ | activation energy ($J/mol$) |
| $f$ | external wetting efficiency ($f = f_d + f_s$) |

| | |
|---|---|
| $F_L$ | liquid feed flow rate (kg/h) |
| H | Henry constant |
| $\Delta H^v$ | water enthalpy of vaporisation (J/mol) |
| $\Delta H_i$ | heat of $i^{th}$ reaction (J/mol) |
| $k_0$ | pre-exponential factor of rate constant of Eq.(1) ($m^3\ s^{-1}\ kg^{-1}$) |
| $k_{gs}$ | gas–solid mass transfer coefficient of oxygen ($m\ s^{-1}$) |
| $k_Ga$ | gas side–liquid volumetric mass transfer coefficient of water vapour ($s^{-1}$) |
| $k_La$ | gas–liquid side volumetric oxygen mass transfer coefficient ($s^{-1}$) |
| $(ka)j_{ll}$ | dynamic–static liquid volumetric mass transfer coefficient of compound j ($s^{-1}$) |
| $k_{jls}$ | j-compound liquid – solid mass transfer coefficient (m/s) |
| $\dot{m}_l$ | mass liquid flow rate (kg/s) |
| $\dot{n}_T^g$ | total molar gas flow rate (mol/s) |
| $\dot{n}_{H_2O}^g$ | molar water vapour flow rate (mol/s) |
| $P^g_{H2O}$ | water vapour pressure (Pa) |
| $P_T$ | total pressure in the reactor (Pa) |
| $Q_G$ | gas feed flow rate at Normal conditions of T and P (Nl/h) |
| r | particle radial dimension (m) |
| $r_i$ | $i^{th}$ reaction rate ($mol\ kg^{-1}\ s^{-1}$) |
| $r_p$ | catalyst particle radius (m) |
| R | universal gas constant ($8.314\ J\ kg^{-1}\ K^{-1}$) |
| $R_j$ | total production rate of compound j ($mol\ kg^{-1}\ s^{-1}$) |
| T | temperature (K) |
| $T_w$ | reactor wall temperature (K) |
| $h_w$ | wall to bed heat transfer coefficient ($W\ m^{-2}\ K^{-1}$) |

| | |
|---|---|
| $u_l$ | liquid superficial velocity (m/s) |
| $u_g$ | gas superficial velocity (m/s) |
| $\dot{V}$ | volumetric flow rate ($m^3$/s) |
| $V_R$ | reactor volume ($m^3$) |
| $W_{cat}$ | catalyst weight (kg) |
| x | liquid molar fraction |
| z | reactor axial dimension (m) |

Greek

| | |
|---|---|
| $\alpha$ | order of reaction of oxygen |
| $\varepsilon_l$ | liquid hold up |
| $\phi'$ | Weisz modulus for pore diffusion based on observed reaction rate |
| $\eta_j$ | effectiveness factor of compound j |
| $\varphi$ | evaporation rate based on reactor length (mol $m^{-1}$ $s^{-1}$) |
| $\mu$ | viscosity (Pa s) |
| $\rho_b$ | apparent bed density (kg/$m^3$) |
| $\rho_l$ | liquid density (kg/$m^3$) |
| $\rho_g$ | gas density (kg/$m^3$) |
| $\rho_p$ | catalyst particle density (kg/$m^3$) |
| $\sigma$ | surface tension (N/m) |
| $\tau$ | space time, defined as $\tau = W_{cat}/F_L$ (h) |

Superscripts

| | |
|---|---|
| ap | apparent |
| d | dynamic liquid |
| g | gas or dry zone |

| | |
|---|---|
| s | static liquid |
| * | on catalyst surface |

Subscripts

| | |
|---|---|
| 0 | at the entrance of the reactor |
| b | bed |
| d | dynamic liquid |
| $H_2O$ | water |
| i | reaction index |
| j | compound index |
| $O_2$ | oxygen |
| p | particle |
| Ph | phenol |
| s | static liquid |
| T | total |
| w | wall |

**Acknowledgements**

We are indebted to the Departament d'Universitats, Recerca i Societat de la Informació de la Generalit de Catalunya for providing financial support to Frank Stüber (ABM/acs/AIRE-CTP2003-3), and the Thailand Research Fund for providing financial support to Somsaluay Suwanprasop through the Royal Golden Jubilee Ph.D. Program (Grant No. PhD/0180/2544).

**References**

(1) Matatov-Meytal, Y.I., Sheintuch, M. Catalytic Abatement of Water pollutants. *Ind. Eng. Chem. Res.* **1987**, 37, 309.

(2) Pintar, A., Besson, A., M., Gallezot, P. Catalytic wet air oxidation of Kraft bleach plant effluents in a trickle bed reactor over a $Ru/TiO_2$ catalyst. *Appl. Cat. B: Environ*. **2001**, 31, 275.

(3) Hussain, S. T., Sayari, A., Larachi, F. Enhancing the stability of Mn-Ce-O WETOX catalysts using potassium. *Appl. Catal. B: Environ*. **2001**, 34, 1.

(4) Suarez-Ojeda, M.E., Stüber, F., Fortuny, A., Fabregat, A., Carrera, J., Font, J. Catalytic wet air oxidation of substituted phenols using active carbon catalyst. *Appl. Catal. B: Environ*. **2005**, 19, 165.

(5) Polaert, I., Wilhelm, A.M., Delmas, H. Phenol wastewater treatment by a two-step adsorption-oxidation process on activated carbon. *Chem. Eng. Sci*. **2002**, 57, 1585.

(6) Mantzavinos, D., Sahibzada, M., Livingston, A.G., Metcalfe, I.S., Hellgardt, K. Wastewater treatment: wet air oxidation as a precursor to biological treatment. *Cat. Today.* **1999**, 53, 93.

(7) Pintar, A., Levec, J. Catalytic liquid-phase oxidation of phenol aqueous solutions. A kinetic investigation. *Ind. Eng. Chem. Res*. **1994**, 33, 3070.

(8) Tukac, V., Vokál, J., Hanika, J. Mass transfer limited wet oxidation of phenol, *J. Chem. Techn. Biotechnol*. **2001**, 76, 506.

(9) Stüber, F., Polaert, I., Delmas, H., Font, J., Fortuny, A. Fabregat, A. Catalytic wet air oxidation of phenol using active carbon: performance of discontinuous and continuous reactors. *J. Chem. Technol. Biotechnol.* **2001**, 76, 743.

(10) Grant, T.M., Judson King, C.D. Mechanism of irreversible adsorption of phenolic compounds by activated carbons. *Ind. Chem. Res.* **1990**, 29, 264.

(11) Stüber, F., Font, J., Fortuny, A., Bengoa, C., Eftaxias, A., Fabregat, A. Carbon materials and catalytic wet air oxidation of organic pollutants in wastewater. *Topics in Cat*. **2005**, in press.

(12) Maugans, C.B., Akgerman, A. Catalytic wet oxidation of phenol in a trickle bed reactor over a $Pt/TiO_2$ catalyst. *Wat. Res.* **2003**, 37, 319.

(13) Eftaxias, A., Larachi, F., Stüber, F. Modelling of trickle bed reactors for the catalytic wet air oxidation of phenol. *Can. J. Chem. Eng*. **2003**, 784.

(14) Suwanprasop, S. Aromatisation of n-hexane and natural gasoline over ZMS-5 zeolite and Wet catalytic oxidation of phenol on fixed bed of active carbon. *Ph. D. thesis Chulalongkorn University (Bangkok, Thailand) and INP Toulouse (France)*, **2005**.

(15) Eftaxias, A. Catalytic Wet Air Oxidation of Phenol in a Trickle Bed Reactor: Kinetics and Reactor Modelling. *Ph. D. thesis Universitat Rovira i Virgili, Tarragona Spain*, **2003**.

(16) Julcour, C., Le Lann, J.M., Wilhelm, A.M., Delmas, H. Dynamics of internal diffusion during the hydrogenation of 1,5,9-cyclododecatriene on $Pd/Al_2O_3$. *Cat. Today.* **1999**, 48, 147.

(17) Van Gelder K.B., Borman P.C., Weenink R.E., Westerterp, K.R. Three-phase packed bed reactor with an evaporating solvent – II. Modelling of the reactor. *Chem. Eng. Sci*. **1990**, 45, 10, 3171.

(18) Reid R.C., Prausnitz J.M., Pauling B.E. The properties of gases and liquids. McGraw-Hill, New York, **1987**.

(19) Diaz M., Vega A., Coca J. Correlation for the estimation of gas-liquid diffusivity. *Chem. Eng. Comm.* **1987**, 52, 271.

(20) Himmelblau, D.M. Solubilities of inert gases in water: 0°C to near the critical point of water. J. Chem. Eng. Data **1960**, 5, 10.

(21) Finlayson, B.A. Nonlinear analysis in chemical engineering. *McGraw-Hill, New York*, **1980**, 113.

(22) Khadilkar, M.R., Wu, Y., Al-Dahhan, M.H., Dudukovic, M.P., Colakyan, M. Comparison of trickle-bed and upflow reactor performance at high pressure: model predictions and experimental observations. *Chem. Eng. Sci.* **1996**, 51, 2139.

(23) Iliuta, I., Larachi, F., Grandjean, B.P.A. Catalyst wetting in trickle flow reactors: a phenomenlogical model. *Chem. Eng. Res. Des.* **1999**, 77, 759.

(24) Al-Dahhan, M.H., Dudukovic, M.P. Catalyst wetting efficiency in trickle-bed reactors at high pressure. *Chem. Eng. Sci.* **1995**, 50, 2377.

(25) Sokolov, V.N., Yablokova, M.A. Thermal conductivity of a stationary granular bed with upward gas-liquid flow. *J. Appl. Chem. USSR* **1983,** 56, 551.

(26) Mariani, N.J., Martinez, O.M., Barreto, G.F. Evaluation of heat transfer parameters in packed beds with cocurrent downflow of liquid and gas. *Chem. Eng. Sci.* **2001**, 56, 5995.

(27) Gianetto, A., Silveston, P.L. Multiphase Chemical Reactors: Theory, Design, Scale-Up. Hardcover, **1986**.

(28) Saada, M.Y. Assessment of interfacial area in co-current two-phase flow in packed beds. *Chimie et industrie, Génie chimique* **1972**, 105, 20, 1415.

(29) Stüber, F. Sélectivité en réacteur catalytique triphasique : analyse expérimentale et théorique d'hydrogénations consécutives en lit fixe catalytique à co-courant ascendant de gaz et de liquide. *Ph. D. thesis INP Toulouse, France* **1995**.

(30) Morsi, B.I. Mass transfer coefficients in a trickle-bed reactor with high and low viscosity organic solutions. *Chem. Eng. J.* **1989**, 41, 41.

(31) Goto, S., Levec, J., Smith, J.M. Mass transfer in packed beds with two-phase flow. *Ind. Eng. Chem. Process. Des. Dev.* **1975,** 14, 4, 473.

(32) Specchia, V., Sicardi, S., Gianetto, A. Absorption in packed towers with concurrent upward flow. *AIChE J.* **1974**, 20, 4, 646.

(33) Michell, R.W., Furzer, I.A. Mixing in trickle flow through packed beds. *Chem. Eng. J.* **1972**, 4, 53.

(34) Dwivedi, P.N., Upadhyay, S.N. Particle-fluid mass transfer in fixed and fluidized beds. *Ind. Eng. Chem. Process. Des. Dev.* **1977**, 16, 2, 157.

(35) Tan, C.S., Smith, J.M. A dynamic method for liquid-particle mass transfer in trickle beds. *AIChE J*. **1982**, 28, 2, 190.

(36) Iliuta, I., Larachi, F., Grandjean, B. P. A. Residence time, mass transfer and back-mixing of the liquid in trickle flow reactors containing porous particles. *Chem. Eng. Sci.* **1999**, 54, 18, 4099.

(37) Hochman, J.M., Effron, E. Two–phase cocurrent downflow in packed beds. *Ind. Eng. Chem. Fund.* **1969**, 8, 1, 63.

(38) Ellman, M.J., Midoux, N., Wild, G., Laurent, A., Charpentier J.C. A new improved liquid hold-up drop correlation for trickle – bed reactors. *Chem. Eng. Sci.* **1990**, 45, 7, 1677.

(39) Saez, A.E., Carbonell, R.G. Hydrodynamic parameters for gas-liquid cocurrent flow in packed beds. *AIChE J.* **1985**, 31, 1, 52.

(40) El-Hisnawi, A.A., Dudukovic, M.P., Mills, P.L. Trickle - bed reactors: dynamic tracer tests, reaction studies, and modeling of reactor performance. *ACS Symp. Ser*. **1982**, 196, 421.

(41) Specchia, V., Baldi, G., Gianetto, A. Solid-liquid mass transfer in concurrent two-phase flow through packed beds. *Ind. Eng. Chem. Proc. Des. Dev.* **1978**, 17, 3, 362.

(42) Yang, X.L., Euzen, J.P., Wild, G. Etude de la rétention liquide dans les réacteurs à lit fixe avec écoulement ascendant de gaz et de liquide. *Entropie* **1989**, 150, 17.

(43) Syaiful. Réacteurs polyphasiques à co-courant ascendant : influence de la viscosité sur les rétentions, dispersions axiales et transfert gaz – liquide. *Ph. D. thesis INP Toulouse, France* **1992**.

(44) Rajashekharam, R., Jaganathan, R., Chaudhari V. A Trickle Bed Reactor Model for Hydrogenation of 2,4 Dinitrotoluene: Experimental Verification. *Chem. Eng. Sci.* **1998**, 53, 4, 787.

**Table 1.**

Reactor type and operating conditions used in the kinetic and scale-up study.

| | Batch Reactor | Small Reactor | Pilot Plant |
|---|---|---|---|
| V, $cm^3$ | 300 | 20 | 600 |
| $D_R$, cm | 6.2 | 1.1 | 2.54 |
| $L_R$, cm | 10 | 20 | 120 |
| $W_{cat}$, kg | $9.10^{-3}$ | $7.10^{-3}$ | 0.325 |
| $d_p$, mm | D[4,3] = 1.0 | 0.5 | D[4,3] = 1.0 |
| $\varepsilon_p$ | 0.53 | 0.53 | 0.53 |
| $C_{Ph,0}$, g/l | 2.5 - 5 | 5 | 5 |
| $P_{O2}$, MPa | 0.1 - 0.35 | 0.1-0.2 | 0.05-0.2 |
| T, ºC | 130 - 160 | 120 - 160 | 120 - 160 |
| $Q_G$, Nl/h | 60 | 9 | 50 - 200 |
| $u_g$, mm/s | --- | 5 | 5 - 25 |
| $F_L$, kg/h | --- | 0.015 - 0.15 | 0.5 - 3.5 |
| $u_l$, mm/s | --- | 0.04 - 0.5 | 0.3 - 2 |
| $\tau$, h | --- | 0.04 - 0.6 | 0.1 - 0.7 |
| G-L flow | --- | up, down | up, down |

**Table 2.**

Values of physical properties in the range of operating conditions used.

| Property | 120 ºC | 140 ºC | 160 ºC | Ref |
|---|---|---|---|---|
| $\rho_{H2O}$ (kg/m$^3$) | 943 | 926 | 908 | 18 |
| $\mu_{H2O}$ (Pa s)x10$^4$ | 2.34 | 1.93 | 1.75 | 18 |
| $\sigma_{H2O}$ (N/m)x10$^2$ | 5.69 | 5.38 | 5.08 | 18 |
| $P^g_{H2O}$ (MPa) | 0.199 | 0.362 | 0.619 | 18 |
| $c_{pl}$ (kJ/kg/K) | 4.24 | 4.28 | 4.34 | 18 |
| $c_{pg}$ (kJ/kg/K) | 1.05 | 1.05 | 1.05 | 18 |
| $\Delta H^v$ (kJ/mol) | 40.2 | 39.13 | 38 | 18 |
| $\Delta H^{com}$ (kJ/mol)[1)] | - 3000 | - 3000 | - 3000 | 18 |
| $D_{O2}$ (m$^2$/s)x10$^{-8}$ | 1.72 | 2.35 | 3.12 | 19 |
| $D_{Phenol}$ (m$^2$/s)x10$^{-8}$ | 0.528 | 0.671 | 0.779 | 18[2)] |
| H (MPa)x10$^{-3}$ | 6.83 | 6.25 | 5.53 | 20 |

[1)] Heat of phenol combustion to form $CO_2$ and $H_2O$.

[2)] Wilke-Chang,1955 in ref. 18.

**Table 3**

Parameter values and correlations used in up- and downflow reactor modelling of pilot plant at: T = 140ºC, $P_T$ = 0.6 MPa, $Q_G$ = 100 Nl/h, $F_L$= 0.5 kg/h.

| Parameter | Downflow operation mode | | Upflow operation mode | |
|---|---|---|---|---|
| $D^{ad}$, $m^2/s$ | $2.2x10^{-5}$ | Michell & Furzer[33], 1992 | $6.4x10^{-5}$ | * |
| $D^{eff}$ ($Ph/O_2$), $m^2/s$ | $1.2/4.2x10^{-9}$ | ** | $1.2/4.2x10^{-9}$ | ** |
| $k_{gs}$, m/s | $3.8x10^{-2}$ | Dwivedi et al.[34], 1977 | ---- | ---- |
| $k^d_{ls}$ ($Ph/O_2$), m/s | $1.4/3.1x10^{-4}$ | Tan & Smith[35], 1982 | $3.2/7.3x10^{-4}$ | Specchia et al. [41], 1978 |
| $k^s_{ls}$ ($Ph/O_2$), m/s | $0.9/2.1x10^{-6}$ | Iliuta et al.[36], 1999 | $0.9/2.1x10^{-6}$ | Iliuta et al.[36], 1999 |
| $(ka)_{ll}$, $s^{-1}$ | $1.0x10^{-2}$ | Hochmann-Effron[37], 1969 | $1.0x10^{-2}$ | Hochmann-Effron[37], 1969 |
| $k_La$, $s^{-1}$ | $8.1x10^{-2}$ | Morsi[30], 1989 | $1.3x10^{-1}$ | Saada[28], 1972 |
| $\varepsilon_{ld}$ | 0.10 | Ellman et al.[38], 1990 | 0.22 | Yang et al.[42], 1989 |
| $\varepsilon_{ls}$ | 0.05 | Saez et al.[39], 1985 | 0.05 | Saez et al.[39], 1985 |
| f | 0.68 (or 1) | El-Hisnawi et al.[40], 1982 | 1.0 | ---- |
| $h_w$ ($W/m^2/K$) | $1.1x10^2$ | *** | $5.1x10^2$ | Sokolov-Yablokova[25], 1983 |

* Axial dispersion estimated from Stüber[29] (correlation derived from Syaiful[43])

** Calculated assuming tortuosity factor = 3

*** Estimated to match the experimental axial temperature profiles (correlation of Mariani et al.[26] is then used to calculate the variation of $h_w$ within the range of operating conditions).

The static, $f_s$, and dynamic, $f_d$, components of the wetting efficiency f were obtained from the approximation of Rajashekharam et al.[44]: $\frac{f_s}{f_d} = \frac{\varepsilon_{ls}}{\varepsilon_{ld}}$

**Table 4**

Influence of $k_La$, $k_Ga$ and $D^{ad}$ on upflow model conversion: comparison with reference case and experimental conversion at $T_{oil}$=140 ºC, $F_L$=0.5 kg/h, $Q_G$=100 Nl/h and $P_{O2}$=0.12 MPa.

| $k_La/k_La_{(Saada)}$ | $k_Ga/k_La$ | $D^{ad}/D^{ad}_{(Stüber)}$ | $\Delta X_{rel}$ (%)* | $\Delta X_{rel}$ (%)** |
|---|---|---|---|---|
| 1 | infinite | 1 | 0 | -5.5 |
| 1 | 5 | 1 | 7.7 | 1.8 |
| 1 | 1 | 1 | 26.7 | 19.7 |
| 0.2 | infinite | 1 | -84.3 | -85.2 |
| 0.2 | 5 | 1 | -56.2 | -58.7 |
| 0.2 | 1 | 1 | -15.5 | -20.1 |
| 5 | infinite | 1 | 30.1 | 23 |
| 5 | 5 | 1 | 31.4 | 24.2 |
| 5 | 1 | 1 | 35.3 | 27.8 |
| 1 | infinite | 4.2 | -4 | -9.3 |
| 5 | 1 | 4.2 | 26.9 | 19.8 |

*relative difference with respect to conversion obtained from simulated reference case of line 1.

**relative difference with respect to experimental conversion.

**Table 5**

Influence of particle wetting efficiency on the simulated outlet phenol concentration in downflow mode: $P_{O2}$=0.12 MPa, $T_w$=140°C, $Q_G$=100 Nl/h, $F_L$=0.5 kg/h, Case: $k_G$a infinite.

| f | 1 | 0.9999 | 0.9 | 0.68* |
|---|---|---|---|---|
| $C_{Ph,out}$ [g/l] | 3.22 | 2.18 | 2.02 | 2.02 |

* calculated from El-Hisnawi[40] correlation.

**List of Figures**

**Figure 1.** Experimental pilot plant reactor (upflow mode).

1 jacketed packed bed column, 2 gas-liquid separator, 3 liquid storage tank, 4 condenser, 5 gas mass-flow controllers, 6 feed tank, 7 balance, 8 dosing pump, 9 sampling device, 10 liquid sample valves, 11 pneumatic valve, 12 expansion vase, 13 gear pump, 14 heater, 15 cooling exchanger, V1-V5 three-way valves for up- or downflow mode.

**Figure 2.** Experimental phenol conversions in downflow mode at 0.1 MPa and 0.2 MPa, and different temperatures: (o) 120 ºC, (□) 140 ºC, (Δ) 160 ºC.

**Figure 3.** Phenol concentration for downflow (open symbols) and upflow (filled symbols) oxidation over active carbon at 0.2 MPa of $O_2$; lines indicate trends.

**Figure 4**. Phenol conversion as a function of liquid space-time for downflow (open symbols) and upflow (filled symbols) at different oxygen partial pressures: (◊) 0.05 MPa, (□) 0.12 MPa, (o) 0.2 MPa; $u_{g,inlet}$ = 1.1–1.2×$10^{-2}$ m/s, $T_w$=140°C. Grey symbols show experimental results without correction by catalyst deactivation.

**Figure 5**. Phenol conversion as a function of liquid space-time for downflow (open symbols) and upflow (filled symbols) at different wall temperatures: (o) 120°C, (□) 140 ºC, (Δ) 160 ºC; $u_{g,inlet}$ = 1.1–1.2×$10^{-2}$ m/s, $P_{O2}$=0.12 MPa. Grey symbols show experimental results without correction by catalyst deactivation.

**Figure 6**. Phenol conversion as a function of gas velocity for downflow (open symbols) and upflow (filled symbols) at different operating conditions ($T_w$=140°C): (◊) $P_{O2}$=0.05 MPa and $F_L$=2 kg/h, (□) $P_{O2}$=0.12 MPa and $F_L$=1 kg/h.

**Figure 7**. Axial temperature profiles for $P_{O2}$=0.12 MPa, $T_w$=140°C, $u_{g,inlet}=1.1\times10^{-2}$ m/s ($Q_G$=100 Nl/h) and $F_L$=1 kg/h. Symbols show experimental results, lines simulation: upflow mode (filled symbols, solid line), downflow mode (open symbols, short dotted line).

**Figure 8.** Upflow outlet phenol concentrations: experimental (symbols) and corresponding simulations for fully wetted catalyst: $k_Ga = k_La$ (solid line), $k_Ga = 5xk_La$ (long dotted line), and instantaneous liquid-vapour equilibrium (short dotted line).

(a) $P_{O2}$=0.12 MPa: (□) $T_w$=140°C ($Q_G$=100 Nl/h*) and (Δ) $T_w$=160°C ($Q_G$=175 Nl/h*)

(b) $P_{O2}$=0.2 MPa, $T_w$=140°C, $Q_G$=100 Nl/h*.

Grey symbols show experimental results without correction by catalyst deactivation.

* same inlet gas velocity: $u_{g,inlet}=1.1\times10^{-2}$ m/s

**Figure 9.** Downflow outlet phenol concentrations: experimental (◊) and corresponding simulations for fully (f=1) and partially (f<1) wetted catalyst: $k_Ga = k_La$ (solid line), $k_Ga = 5xk_La$ (long dotted line), and instantaneous liquid-vapour equilibrium (short dotted line).

$P_{O2}$=0.12 MPa, $T_w$=140°C, $Q_G$=100 Nl/h.

Grey symbols show experimental results without correction by catalyst deactivation.

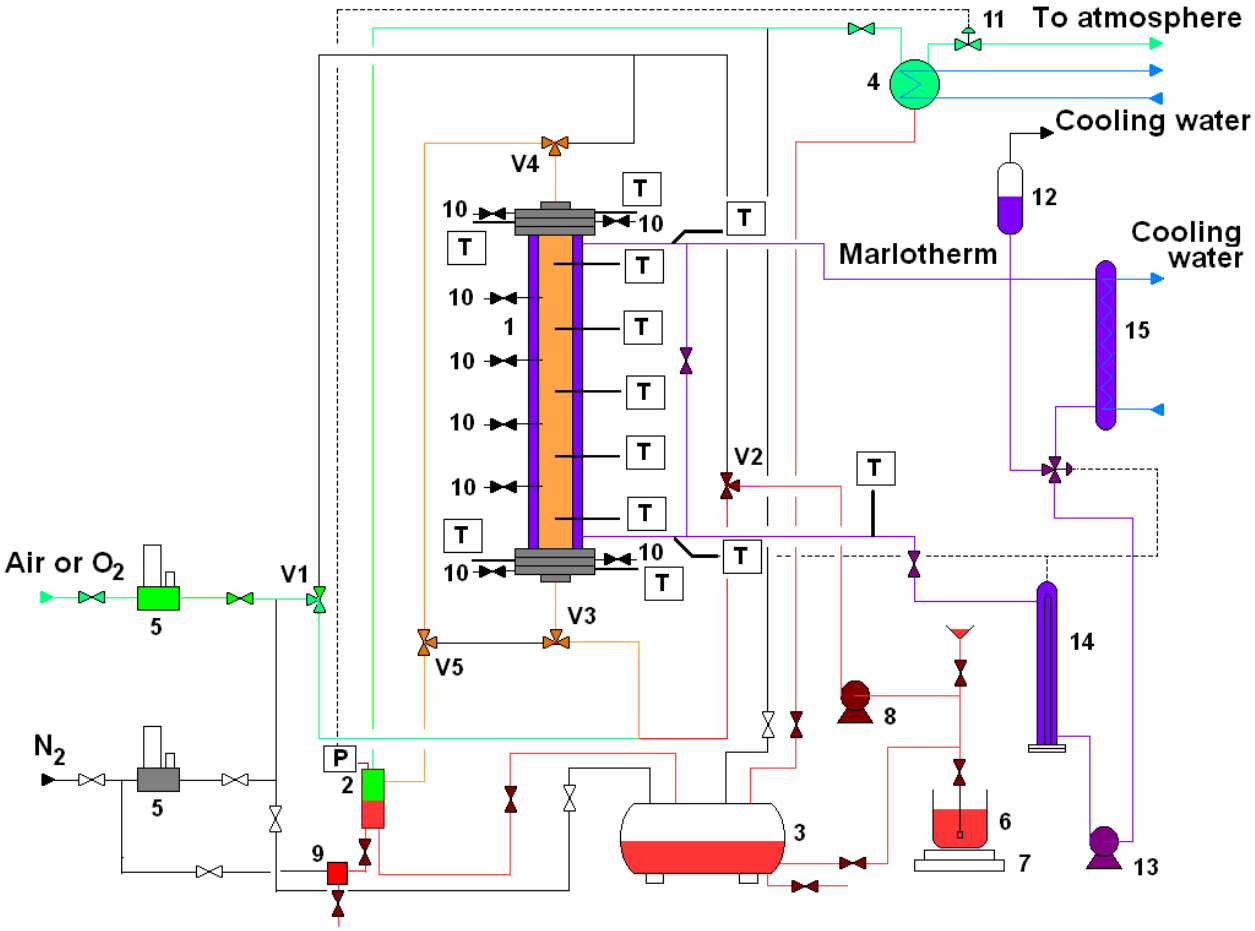
11
To atmosphere
4
Cooling water
12
V4
T
10
Marlotherm
Cooling
water
15
1
V2
Air or $O_2$
V1
5
V3
V5
14
8
$N_2$
P
2
3
6
9
7
13

**Figure 1**

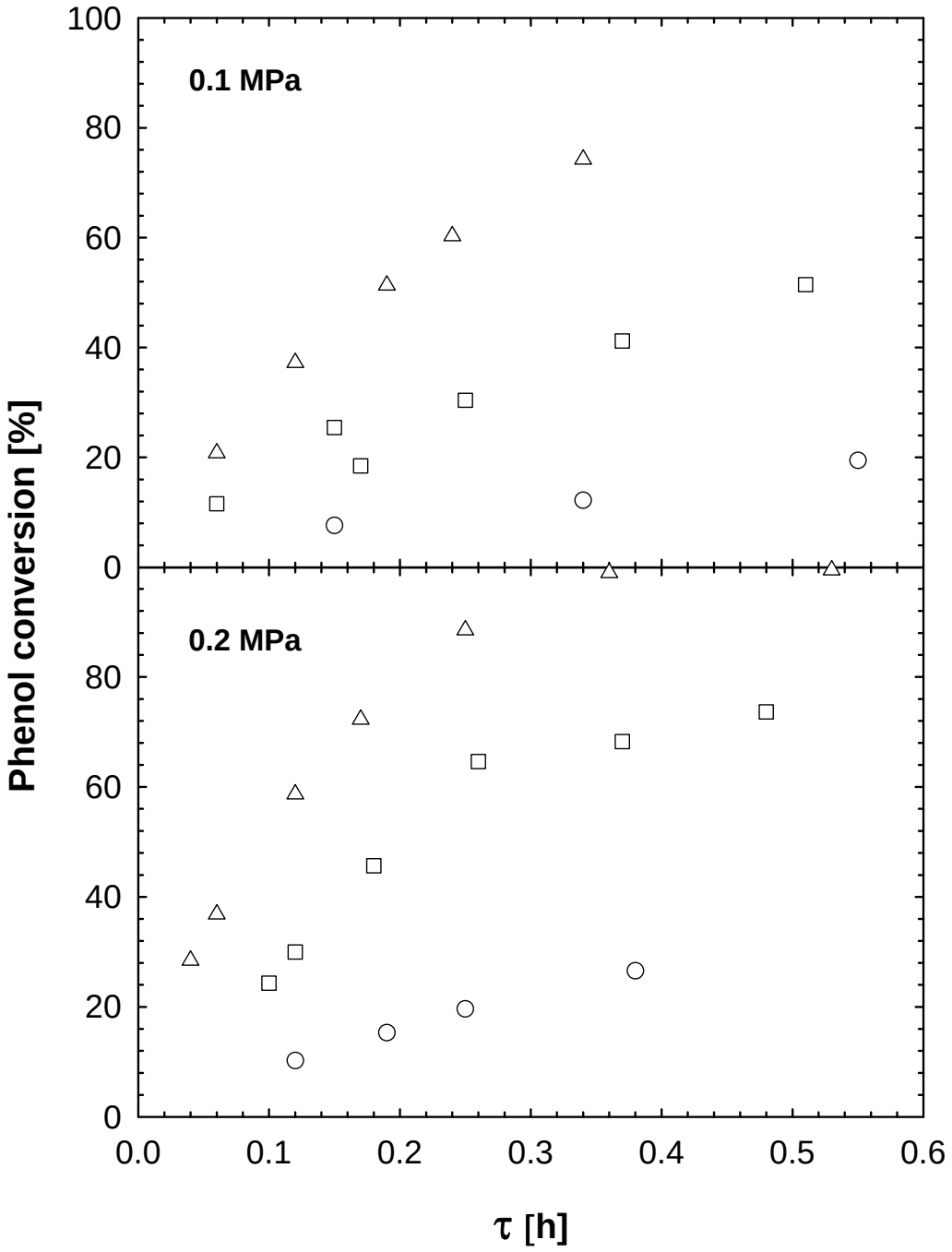
0.1 MPa
0.2 MPa
Phenol conversion [%]
τ [h]
0
20
40
60
80
100
0.0
0.1
0.2
0.3
0.4
0.5
0.6

**Figure 2**

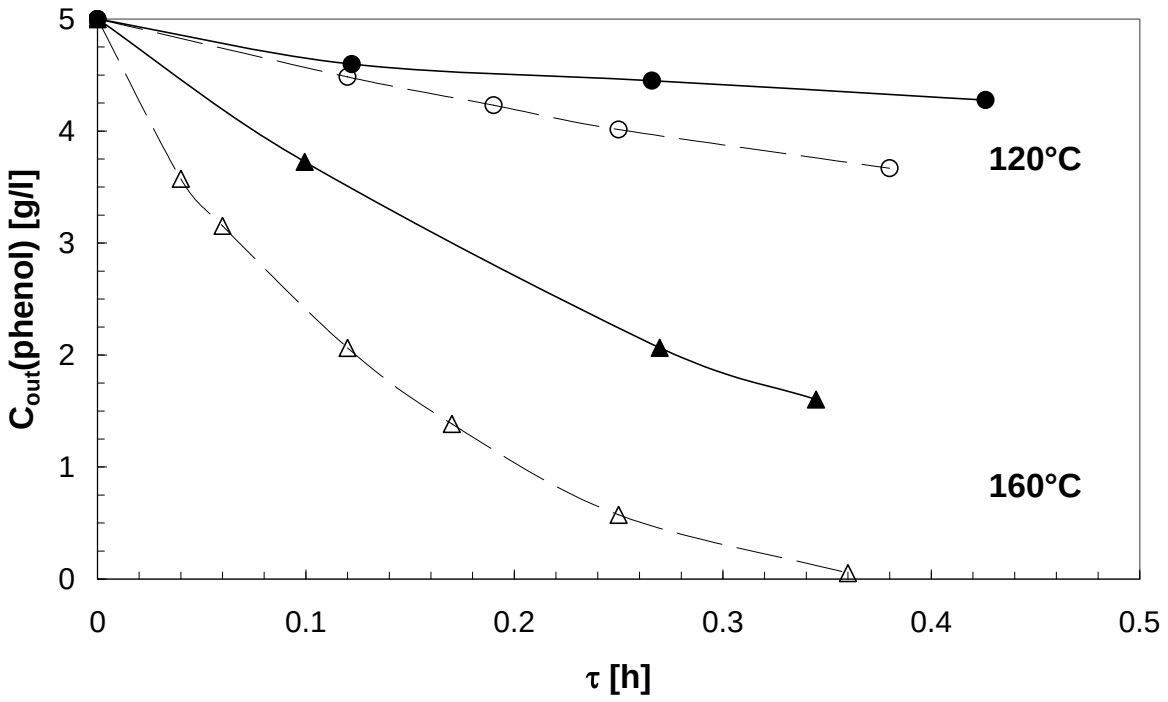


**Figure 3**

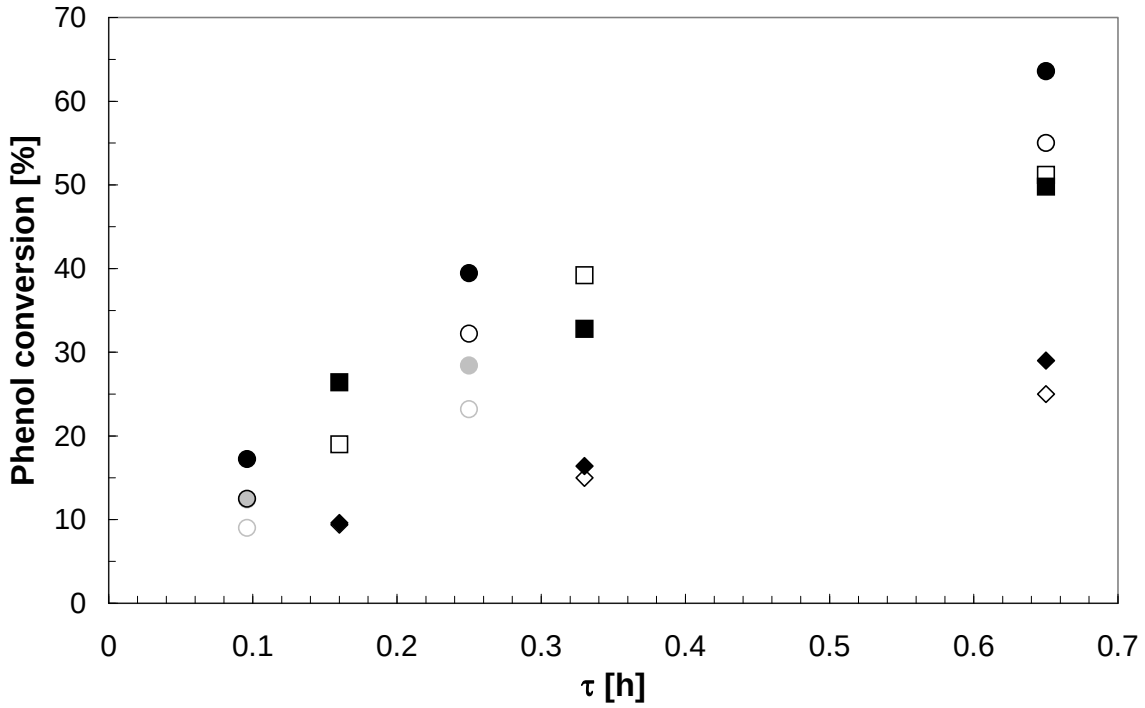


**Figure 4**

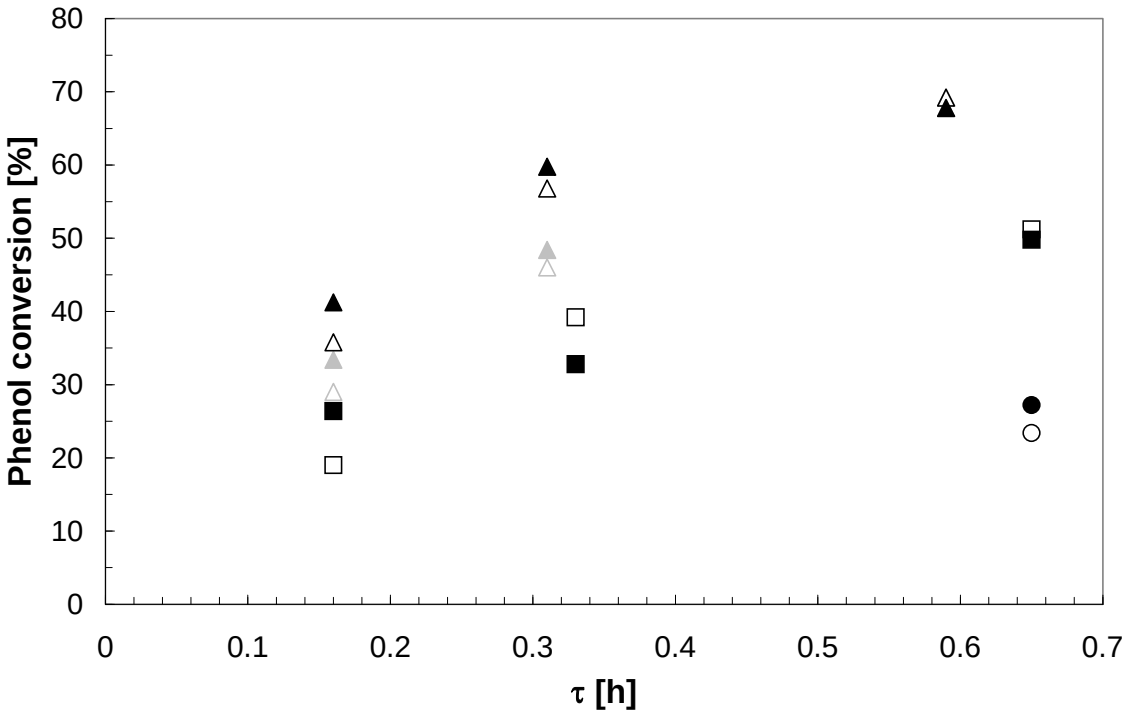
Phenol conversion [%]
80
70
60
50
40
30
20
10
0
0
0.1
0.2
0.3
0.4
0.5
0.6
0.7
τ [h]

**Figure 5**

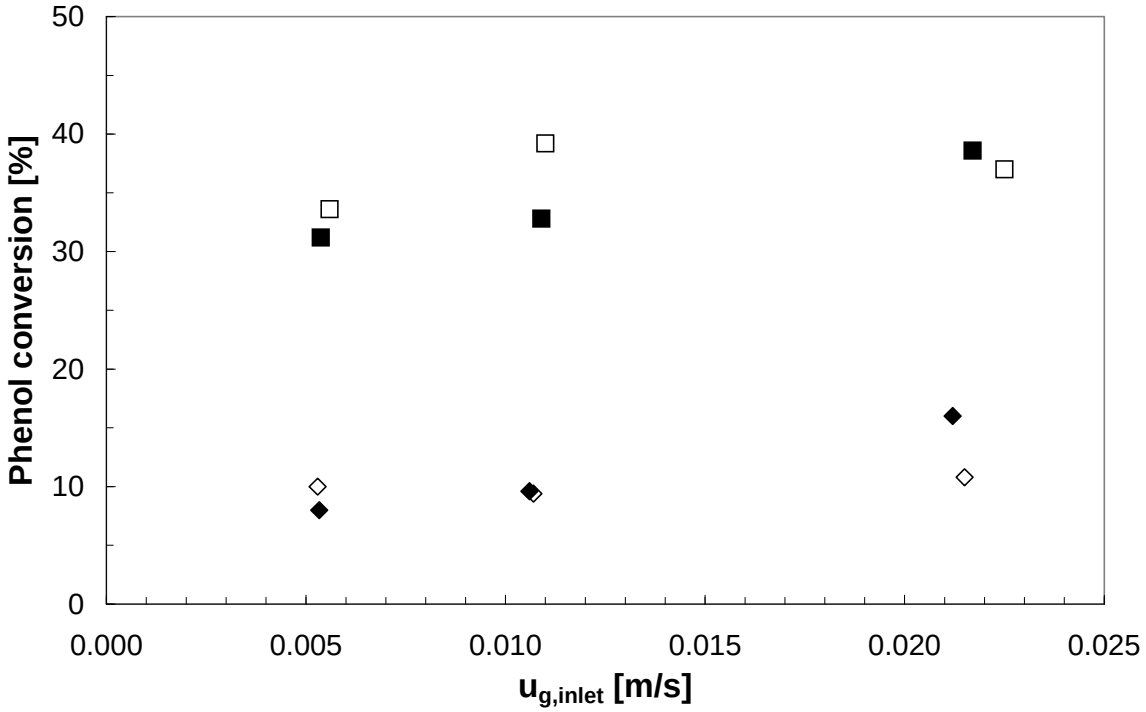
Phenol conversion [%]
50
40
30
20
10
0
0.000
0.005
0.010
0.015
0.020
0.025
$u_{g,inlet}$ [m/s]

**Figure 6**

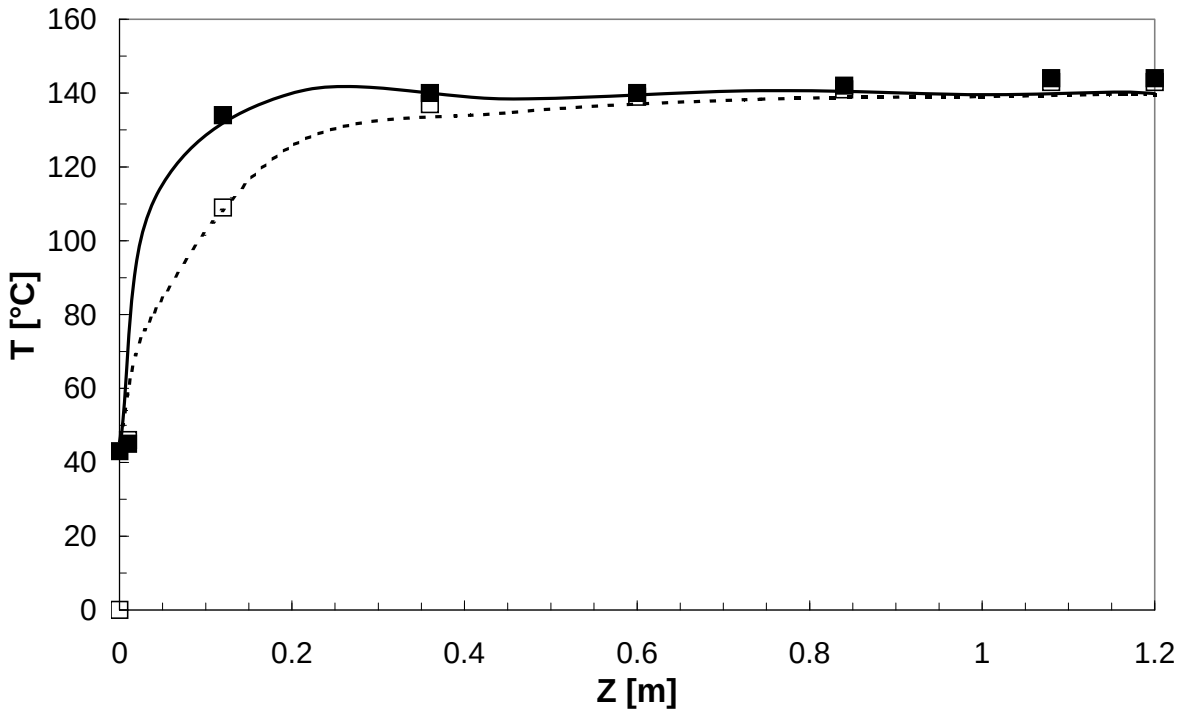


**Figure 7**

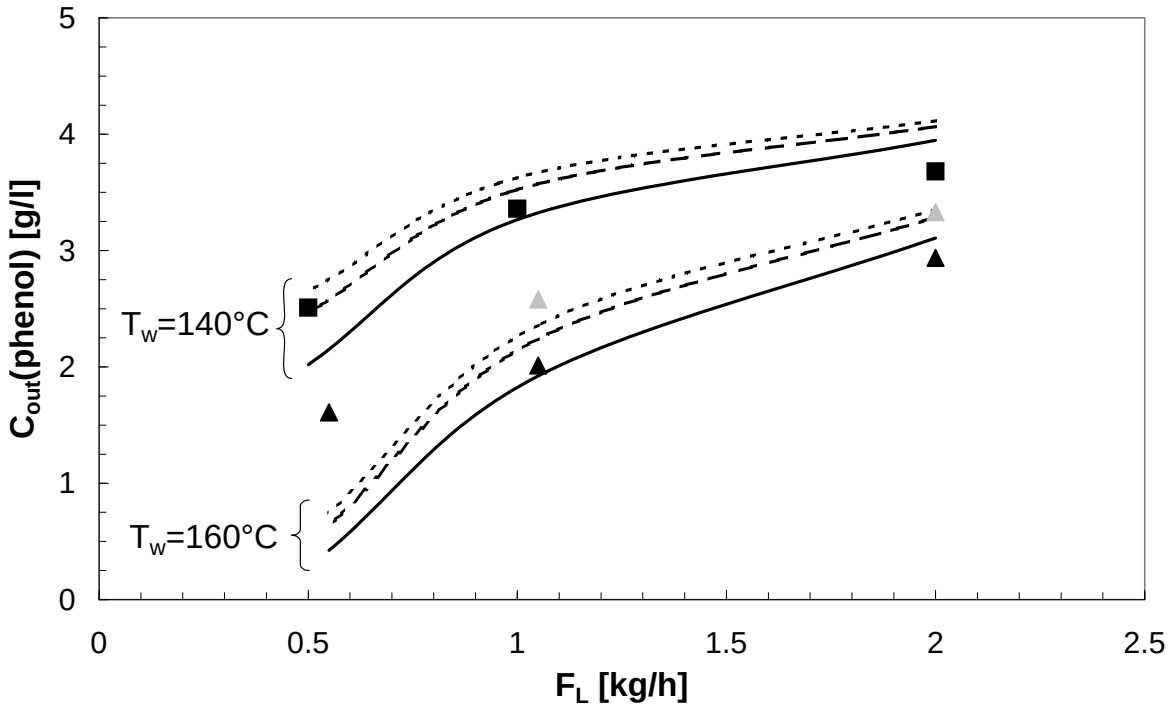


**Figure 8 a**

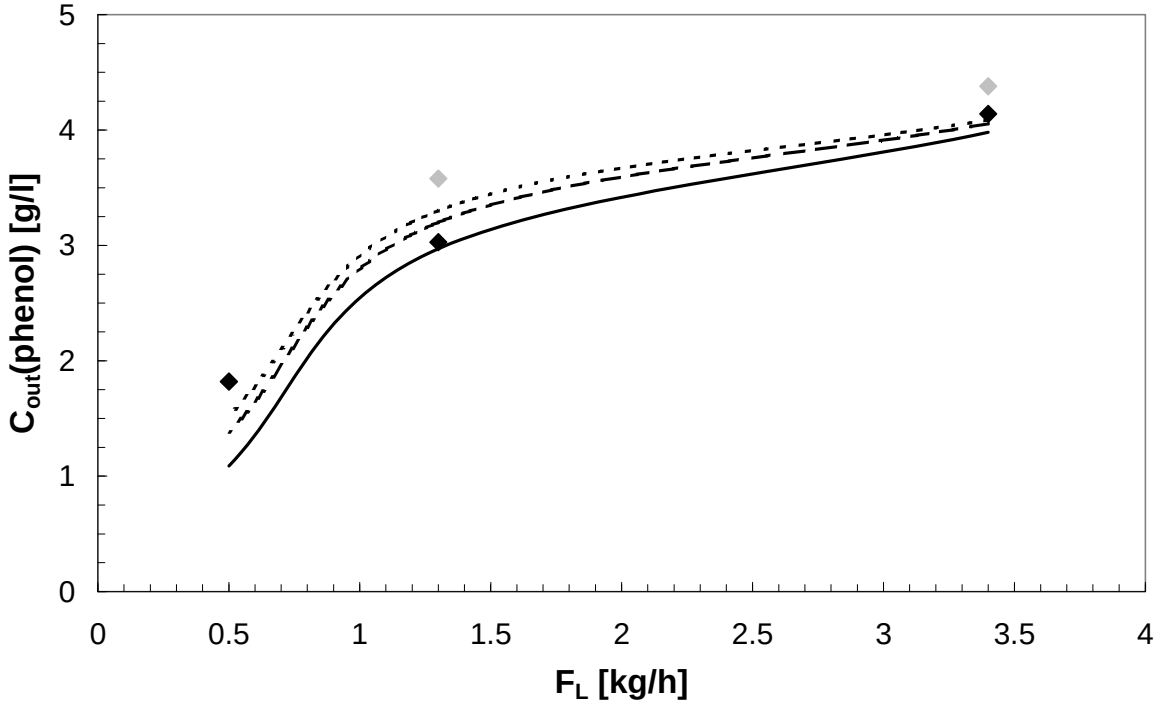


**Figure 8 b**

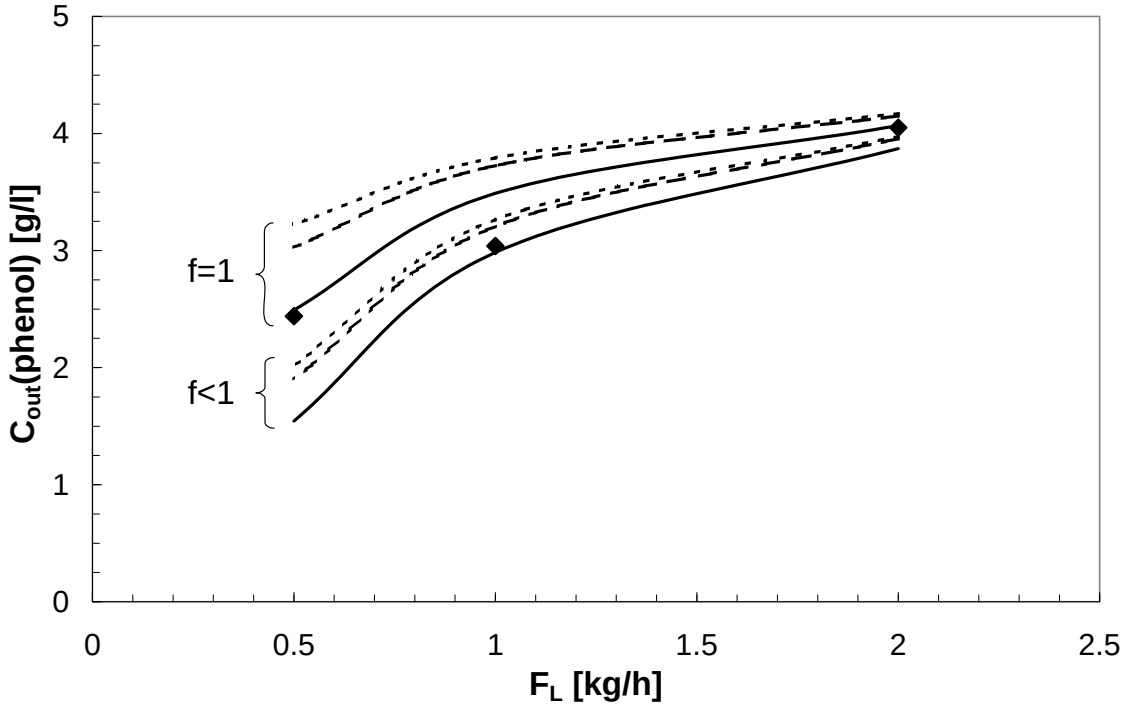


**Figure 9**